Accepted Manuscript

Structure-activity relationship study and biological evaluation of SAC-Garlic acid conjugates as novel anti-inflammatory agents

Jingjie Bi, Wenqing Wang, Junxi Du, Kun Chen, Kui Cheng

PII: S0223-5234(19)30586-0

DOI: https://doi.org/10.1016/j.ejmech.2019.06.059

Reference: EJMECH 11462

To appear in: *European Journal of Medicinal Chemistry*

Received Date: 11 April 2019

Revised Date: 17 June 2019

Accepted Date: 21 June 2019

Please cite this article as: J. Bi, W. Wang, J. Du, K. Chen, K. Cheng, Structure-activity relationship study and biological evaluation of SAC-Garlic acid conjugates as novel anti-inflammatory agents, *European Journal of Medicinal Chemistry* (2019), doi: https://doi.org/10.1016/j.ejmech.2019.06.059.

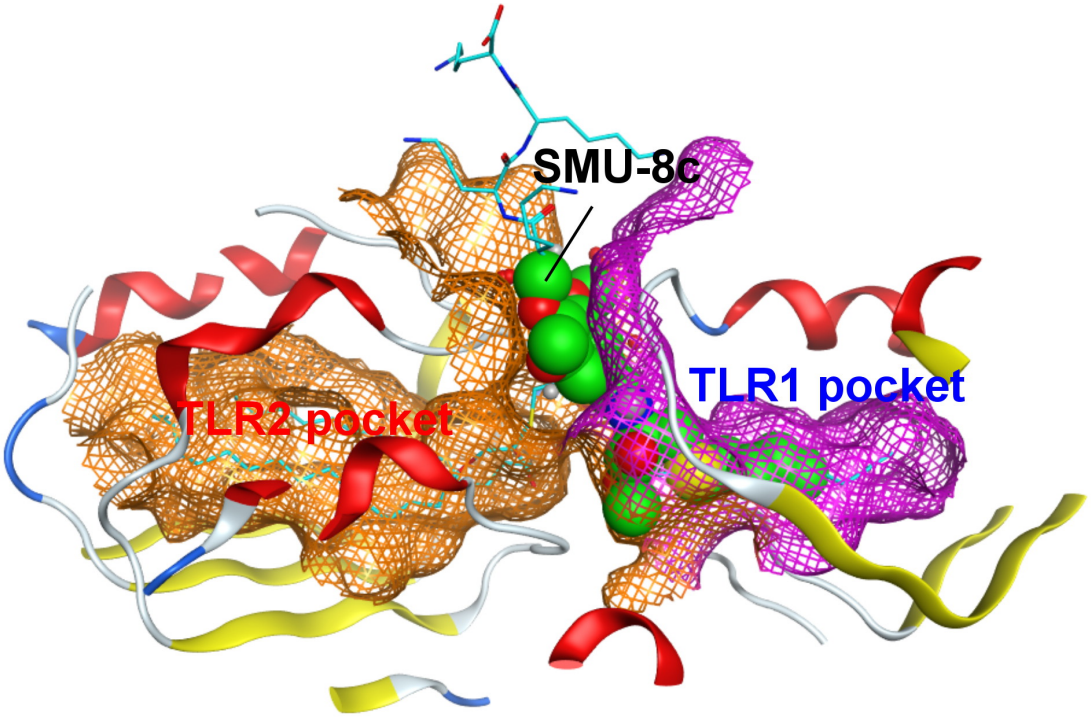

Structure-activity relationship study and biological evaluation of SAC-Garlic Acid conjugates as novel anti-inflammatory agents

Jingjie Bi [a], Wenqing Wang [a], Junxi Du [b], Kun Chen [b, *] and Kui Cheng [a, *]

[a]*Guangdong Provincial Key Laboratory of New Drug Screening and Guangzhou Key Laboratory of Drug Research for Emerging Virus Prevention and Treatment, School of Pharmaceutical Sciences, Southern Medical University, Guangzhou, 510515, China.*

[b]*The Joint Research Center of Guangzhou University and Keele Univeristy for Gene Interference and Application, School of Life Science, Guangzhou University, Guangzhou, 510006, China.*

∗ Corresponding author. Tel.: +86-20-61647192; fax: +86-20-61648533; e-mail: chengk@smu.edu.cn

∗ Corresponding author. Tel.: +86-20-39366915; fax: +86-20-39366915; e-mail: kchen@gzhu.edu.cn

Abstract:

A series of S-allyl-L-cysteine (SAC) with garlic acid conjugates as anti-inflammatory agents were designed and synthesized. Among the 40 tested compounds, SMU-8c exhibited the most potent inhibitory activity to Pam_3CSK_4-induced nitric oxide (NO) in RAW264.7 macrophages with IC_{50} of 22.54 ± 2.60 μM. The structure-activity relationship (SAR) study suggested that the esterified carboxyl group, carbon chain extension and methoxylation phenol hydroxy could improve the anti-inflammatory efficacy. Preliminary anti-inflammatory mechanism studies showed that SMU-8c significantly down-regulated the levels of Pam_3CSK_4 triggered TNF-α cytokine in human THP-1 cells, mouse RAW 264.7 macrophages, as well as in *ex-vivo* human peripheral blood mononuclear cells (PBMC) with no influence on cell viability. SMU-8c specifically blocked the Pam_3CSK_4 ignited secreted embryonic alkaline phosphatase (SEAP) signaling with no influence to Poly I:C or LPS triggered TLR3 or TLR4 signaling. Moreover, SMU-8c suppressed TLR2 in HEK-Blue hTLR2 cells and inhibited the formation of TLR1-TLR2, and TLR2-TLR6 complex in human PBMC. In summary, SMU-8c inhibited the TLR2 signaling pathway to down-regulate the inflammation cytokines, such as NO, SEAP and TNF-α, to realize its anti-inflammatory activity.

Keywords: SAC-Garlic acid conjugates; Structure-activity relationship; Anti-inflammatory; Toll-like receptor 2.

1. Introduction

Garlic acid is a type of phenolic acid, and has been widely found in natural plants, such as Chinese nutgall, rhubarb, lacquer tree, and some fruits [1, 2]. Many drugs contain a skeleton of methylated garlic acid, such as reserpine, deserpidine, and trimethoprim [3, 4]. Garlic acid has been shown to have beneficial effects on anti-inflammation, vascular calcification, and metabolic diseases, as well as scavenges free radicals and regulates different intracellular signaling pathways [5]. Recent

researches have demonstrated that garlic acid can down-regulate the expression of matrix metalloproteinase 2 and matrix metalloproteinase 9 then inhibit tumor growth [6, 7]. It was also reported as an antagonist of semen amyloid fibrils to attenuate HIV-1 infection [8], and interacted with a-synuclein, associated with Parkinson's disease, to prevent the structural change required for its fibril formation [9]. In addition, garlic acid exhibited that it can suppress the inflammatory reaction by inhibiting activation of the p65-NF-kB and IL-6/STAT3 pathways [10].

On the other hand, S-allyl-L-cysteine (SAC) and its modifications S-propargyl-L-cysteine (SPRC) (Fig. 1), or SPRC-Leonurine complex revealed exciting anti-inflammatory, anti-atherogenic effects by decrease the nitric oxide (NO) on macrophages and endothelial cells [11], as well as protective effects on acute myocardial ischaemia through regulating cysthathionine-glyase pathway [12]. SAC is also a well-known bioactive component of the aqueous garlic, exhibiting NF-κB inhibition effect in T cells [13]. Thus, the selective inhibition of NO and NF-κB may contribute to anti-inflammatory effect and prevention of atherosclerosis. SAC or SPRC-Leonurine complex, a new class of multifunctional antimyocardial ischaemia agents, displayed potent cardioprotective effect at lower molar concentration [14, 15].

Incorporation of two mutually complementary biological active by conjugating into one has been widely used in drug design. Recently, researcher attempted to integrate the chemical features of garlic acid and methyl-L-leucine to yield a novel garlic acid-L-leucine (GAL) conjugate. The results suggested that GAL conjugate may serve as a new scaffold compound for the development of new anti-inflammatory drugs [16]. Garlic acid-β-D-glucose conjugates (BGG), a major component of the Emblica officinalis medicinal plant, demonstrated specific inhibition to inflammatory diseases, particularly diabetic eyes diseases [17]. Garlic acid-Quercetin conjugate increased both the mRNA and protein levels of HO-1 in RAW cells through MAPK/Nrf2 pathway [18], and Garlic acid-triphenylphosphonium lipophilic cations showed significantly antiproliferative effect *in vivo* [19]. Garlic acid and rivastigmine hybrid GA2 efficiently prevented the self-mediated Aβ aggregation as a new approach against Alzheimer's disease [20].

Toll-like receptors (TLRs) is one of the pattern recognition receptors, associated with variety of immune-related diseases [21-30]. Inspired by above paradigms, as well as our continued work to develop new modulators of TLRs [31-35], in the present study, a series new GA-SACs conjugates were developed and their inhibitory activity to the proinflammatory cytokines were also evaluated, including NO, TNF-α and SEAP. Next, the preliminary anti-inflammatory mechanisms of the most potent compound were further explored.

2. Design idea

In view of the operability of the combination and the stability of the forming compound, we adopted a binding strategy for forming an amide bond between SAC and garlic acid, and got a new scaffold SGA (Fig. 2). Three positions in SGA were investigated for the structure-activity relationship (SAR). First, based on the allyl substitution of SAC (blue color), we varied the length of the carbon chain, including1-butenyl or 1-pentenyl substitution. Replacing the allyl by a propynyl group made the structure more linear. Considering the electronic and steric effects, we replaced the allyl group with a more sterically hindered and more rigid benzyl group. In the second part (purple color), we methylated the SAC carboxyl group to make the compound more hydrophobic. In the third part (red color), we investigated the effect of the hydroxyl groups on the activity according the availability of the substrate. A series of compounds with hydroxy substitution at the 4th position or the 3rd, 5th positions, or trimethoxy group substitution at the 3rd, 4th, and 5th positions were investigated.

3. Results and discussion

These potential anti-inflammatory agents were prepared by following Scheme 1. All targeted compounds were test for their anti-inflammatory activity by secreting pro-inflammatory NO in RAW 264.7 cells. To monitor the activation of inflammatory state, the TLR2 agonist Pam_3CSK_4 was used as the positive control.

3.1. Structure-activity relationship study.

The IC_{50} results of SGA and its derivatives in RAW 264.7 cells were illustrated in Table 1. Comparison of 1a-f and 2a-f, we knew that SAC and its derivatives had no nitric oxide inhibitory activity even up to 150 μM. Methylated the carboxyl group enhanced its anti-inflammatory activity. Compound 2c was better than others (2a to 2f), indicating that the hydrophobic effect was helpful for the activity. Similar result was also observed between compound 3a-c and 6a. When the -OH substitutions at the 4th position, or the 3rd, 5th positions of the benzene ring were removed, the activity decreased. Meanwhile, the inhibitory activity was improved when trimethoxy group substitutions showing up at the 3rd, 4th, and 5th positions. Secondly, among SGA and its derivatives (8a-f, 10a-r), as we expected, the compound SMU-8c, which was a combination of 2c and 6a by forming an amide bond, exhibited the best inhibitory activity with IC_{50} of 22.54 ± 2.60 μM (Fig. 3A and Table 1). SMU-8c was much better than SAC (1a, IC_{50} > 150 μM) and garlic acid (3a, IC_{50} of 69.25 ± 4.22 μM), as well as much better than 2a and garlic acid conjugated compound 10a. SAR studies found that when an allyl substitution was increased to 1-butenyl or 1-pentenyl, the inhibitory activity was increased follow the carbon chain extension (8a-c, 10a-c, 10g-i, 10m-o). At the same time, when we replaced the first part of 1-pentenyl with the linear group propynyl (8d, 10d, 10j, 10p), the activity of the compounds decreased dramatically. This indicated that the steric hindrance of the substituents greatly influence their inhibitory activity. This result was further confirmed by replacing propynyl with a benzyl group or 4-fluorobenzyl group (8e-f, 10e-f, 10k-l, 10q-r), and the inhibitory activity of these compounds increased. Moreover, the activities of the benzyl compounds with an electron-withdrawing substitution in the para position (8e, 10e, 10k, 10q) were more potent than that with no substitutions (8f, 10f, 10l, 10r). While the activity of all these compounds were not superior to that of 1-pentenyl substituted compounds. From above results we can conclude that the first part (I) of the substituent favors certain steric hindrance and flexibility chain, while the second (II) and third (III) part like the hydrophobic substitutions and were necessary for the inhibitory activity.

3.2. Target validation of SMU-8c

SMU-8c inhibited the inflammation cytokine nitric oxide on RAW 264.7 cells with TLR2 agonist Pam_3CSK_4 as the positive control. To confirm this effect was associated with TLR2, SMU-8c was test for TLR2 inhibition in HEK-Blue hTLR2 cells. This cell line was obtained by co-transfection of the human TLR2 and SEAP (secreted embryonic alkaline phosphatase) genes into HEK293 cells. Additionally, the CD14 co-receptor gene was also transfected into these cells to enhance the TLR2 response. TLR2 specific ligand Pam_3CSK_4 can activate the NF-kB and AP-1 signaling pathway to induce the SEAP signaling in HEK-Blue hTLR2 cells. Similar to the results observed on RAW 264.7 cells, SMU-8c suppressed SEAP signaling in a concentration dependent manner in HEK-Blue hTLR2 cells, with almost 50 percent inhibition at 25 μM. SAC as a negative control showed no inhibition (Fig. 3B). So, the optimized compound SMU-8c was selected out for further assays.

3.3. *In vitro* cytotoxicity studies

In vitro toxicity of the compound was evaluated by a MTT colorimetric method in RAW 264.7 cells. From the MTT assay results (Fig. 4), we can confirm that SMU-8c had no significant cytotoxicity problem as concentration up to 100 μM. Considering compound SMU-8c having the lowest IC_{50}, high inhibitory activity, low toxicity, as well as appropriate molecular weight, it might own the higher drug-like potential ability. Thus, compound SMU-8c was picked out to evaluate its selectivity and other potential mechanisms.

3.4. Specificity assays

From the previous experiments, we knew that SMU-8c can inhibit the SEAP signal stimulated by Pam_3CSK_4 on HEK-Blue hTLR2 cells. But TLR family can recognize a large range of ligands, so we conducted a selectivity examination to investigate whether SMU-8c could specifically inhibit TLR2 signaling. The targets included TLR1/2, TLR2/6, TLR3, and TLR4, and their native ligands were Pam_3CSK_4,

Pam_2CSK_4, Poly I:C, and LPS, respectively. As shown in Fig 5, both TLR1/2 and TLR2/6 were inhibited (Fig. 5A), which had no influence on TLR3 and TLR4 (Fig. 5B and 5C). These results suggested that SMU-8c was an antagonist of TLR2.

We also evaluated whether SMU-8c influences the TLR2 expression in the whole-cell environment. HEK-Blue hTLR2 cells, which overexpress the human TLR2, were stimulated with Pam_3CSK_4 (50 ng/mL). Cell lysates were subjected to immunoprecipitation and immuno-detected using TLR2 antibody. As illustrated in Fig. 6A, the TLR2 protein upregulated when the Pam_3CSK_4 added and this upregulation could be inhibited by SMU-8c in a dose-dependent manner. TLR2 protein was suppressed more than 90% at 12.5 μM. A co-immunoprecipitation assay was also conducted to validate the effect of compound SMU-8c on TLR1–TLR2, TLR2–TLR6 heterodimerization, as well as TLR2 and its adaptor protein MyD88 in cellular level. Human peripheral blood mononuclear cells (PBMC) pre-treated with compound SMU-8c were stimulated with Pam_3CSK_4 or Pam_2CSK_4 and TLR1–TLR2, TLR2-TLR6, TLR2-MyD88 complexes were pulled down using protein A agarose beads coated with anti-TLR2 antibodies. The complexes were then analyzed by Western blotting using anti-TLR1, anti-TLR2, anti-TLR6, anti-MyD88 antibodies (Fig. 6B, C). In the absence of Pam_3CSK_4 (TLR1/2 ligand) or Pam_2CSK_4 (TLR2/6 ligand), less TLR1, TLR6, MyD88 were detected in the immunoprecipitates, while the TLR1–TLR2, TLR2–TLR6, and TLR2-MyD88 complexes were detected with the present of the ligands. Decreased TLR1, TLR6, MyD88 were found in immunoprecipitates from Pam_3CSK_4 or Pam_2CSK_4-treated cells in a dose-dependent manner, indicating that TLR1–TLR2 heterodimerization, TLR2–TLR6 heterodimerization, TLR2-MyD88 complexes formation were inhibited and were pulled down together. These results indicate that SMU-8c, as an antagonist of TLR2, is capable of inhibit the TLR2 on the cell surface and downregulate Pam_3CSK_4 or Pam_2CSK_4 triggered TLR2 protein and its adaptor protein MyD88.

3.5. Downstream signaling evaluation

We performed ELISA to analyze the effect of compound SMU-8c on

downstream signaling. In our experiments, we tested the inflammatory cytokine TNF-α to characterize the compound's inflammatory inhibition ability. The data in RAW 264.7 cells showed that SMU-8c can dose dependently decrease the Pam_3CSK_4-triggered TNF-α signaling, with 25 μM almost inhibiting 50% TNF-α signaling (Fig. 7A), which was similar to results observed in human THP-1 monocyte cells (Fig. 7B). In *ex-vivo* human peripheral blood mononuclear cells (PBMC) experiment, the inhibition rate of SMU-8c at 12.5 μM has exceeded 95%, which showed the compound maybe more potent in the *ex-vivo* model (Fig. 7C).

3.6. Molecular docking studies of SMU-8c

To examine possible explanations for the significantly TLR2 inhibition potency in human cells, we explored the predicted binding mode(s) of compound SMU-8c with the TLR1/TLR2 complex by conducting molecular docking experiments in the human protein crystal complex (PDB 2Z7X). We selected the most favorable energy configuration of SMU-8c (shown in orange) and compared the binding of Pam_3CSK_4 (shown in purple) bound to the complex (Fig. 8). Of particular interest is that SMU-8c is well binding to the interface of TLR1 (A) and TLR2 (B), tightly fits into the binding site of Pam_3CSK_4 and TLR1 and TLR2, and shows significant interaction with the important residues, such as Gly313, Gln316 on TLR1 and Phe349 on TLR2 (Fig. 8). The long chain of olefins binds well to the hydrophobic cavity in which Pam_3CSK_4 binds to TLR1, which probably explains why carbon chain elongation has a certain increase in activity. The methoxy group has a hydrophobic interaction with the active site of TLR2 which probably explain that the activity is significantly reduced when the methoxy groups changed into hydroxyl groups. The top three active compounds (SMU-8c, 8b and 8f) also showed similar binding mode to the protein-protein interaction domain of TLR1/2 (Fig. S1).

4. Conclusion

In conclusion, a series of SGA or SGA derivatives have been designed and

synthesized based on our continued work to develop new anti-inflammatory reagents. SAR studies of a series compounds yield a new SAC and garlic acid conjugate SMU-8c with the most anti-inflammatory potential. Specificity experiments confirmed that SMU-8c had low toxicity and selectivity to TLR2, with no influence to TLR3 and TLR4. Immunoprecipitation assays confirmed that SMU-8c could inhibit the TLR2 protein, and influence the formation of TLR1-TLR2, TLR2-TLR6 as well as TLR2-MyD88 complex to downregulate the downstream signaling. Following ELISA result showed that SMU-8c can not only inhibit the TNF-α in the mouse macrophages, but also inhibit the TNF-α in human THP-1 monocytes, as well as in human PBMC cells. In summary, our study has provided a novel, drug-like and potent nature product conjugate small molecular as anti-inflammatory reagents by inhibit TLR2, which might be further explored involving some diseases associated with inflammation or tumor.

5. Experimental section

5.1. Chemistry

Commercially available chemicals were purchased from Macklin or Sigma-Aldrich and without further purification. ^{1}H NMR and ^{13}C NMR spectra of all compounds were obtained with a Bruker Advance 400 spectrometer at 400 MHz in a solution of $CDCl_3$, DMSO-d_6 or D_2O. Data for ^{1}H NMR spectra were reported as follows: chemical shift (δ ppm), multiplicity, coupling constant (Hz), integration. Multiplicities were reported as follows: s=singlet, d=doublet, t=triplet, q=quartet, m=multiplet. All compounds were routinely checked by thin-layer chromatography (TLC). UV light was used to examine the spots. Low-resolution mass spectra ESI-MS were recorded on a Waters ZQ 4000 apparatus. Evaporation was performed in vacuum (rotating evaporator). Sodium sulfate was always used as the drying agent.

The general synthetic procedures followed for the synthesis of final compounds. Briefly, the brominated unsaturated alkane or aromatic hydrocarbon were reacted with L-cysteine in $NH_3 \cdot H_2O$ to obtain compounds 1a-f. Then, in a methanol solution, the methyl esterified products 2a-f were obtained under the catalysis of $SOCl_2$. The

reaction of a hydroxy-substituted benzoic acid compounds 3a-c with acetic anhydride gived a hydroxyacetylated protective products 4a-c. Compounds 8a-f or 9a-r were prepared by the reaction of different substituted benzoyl chloride compounds 5a-c or 7a，freshly prepared by treatment of $SOCl_2$, and the amine-derivatives. Finally, deacetylation protection in $NaHCO_3$ (1M), yielded the final compounds 10a-r.

General procedure for the synthesis of compounds 1a-f

3-bromoprop-1-ene (3271 mg, 20.490 mmol) was added dropwise to a solution of L-cysteine (3000 mg, 24.789 mmol) in $NH_3 \cdot H_2O$ (8 ml), pre-cooled for 15 minutes in ice water. The reaction mixture was stirred for 12h, after which the solvent was removed using a rotary evaporator under 40 ^oC, and any residual 3-bromoprop-1-ene was removed by washing with ethanol. The crude product was recrystallized in a mixed solution of water:ethanol = 2:3. After filtration, the pure product was obtained and dried in an oven under 40 ^oC. Yielding 65% compound 1a (2595 mg) as a white solid. Compounds 1b-f were synthesized following the procedure of preparation 1a.

General procedure for the synthesis of compounds 2a-f

$SOCl_2$ (2038 mg, 17.132 mmol) was added dropwise to a solution of 1a (1000 mg, 6.209 mmol) in CH_3OH (3167 mg, 98.845 mmol), pre-cooled for 15 minutes in ice water. The reaction mixture was stirred for 12h. The solvent was removed under reduced pressure. The crude product was recrystallized in CH_2Cl_2 and dried under vacuum. Yielding 93% compound 2a (1011 mg) as a white solid. Compounds 2b-f were synthesized following the procedure of preparation 2a.

General procedure for the synthesis of compounds 4a-c

Garlic acid (2000 mg, 11.763 mmol) was dissolved in acetic anhydride (7205 mg, 70.578 mmol). The solution was then heated under reflux at 130 ^oC for 4 h, after which the deionized water (4 ml) was add to the solution to remove the unreacted acetic anhydride. The solvent was removed using a rotary evaporator under reduced pressure to yield white solid. The product was recrystallized in CH_2Cl_2 and dried

under vacuum. Yielding 95% compound 4a (3308 mg) as a white solid. Compounds 4b-c were synthesized following the procedure of preparation 4a.

General procedure for the synthesis of compounds 5a-c, 7a

3,4,5-triacetoxybenzoic acid 4a (2000 mg, 6.756 mmol) was dissolved in $SOCl_2$ (8000 mg, 67.244 mmol). The solution was then heated under reflux at 78 ^oC for 4 h. The solvent was removed using a rotary evaporator under reduced pressure to yield white solid. Yielding 99% compound 5a (2100 mg) as a white solid. Compounds 5b-c and 7a were synthesized following the procedure of preparation 5a.

General procedure for the synthesis of compounds 8a-f, 9a-r

To a solution of methyl (S)-2-aminopent-4-enoate 2a (600 mg, 4.648 mmol) in CH_2Cl_2 (4 mL) was added triethylamine (1500 mg, 14.823 mmol). The mixture was allowed to stir 30 min. 3,4,5-trimethoxybenzoyl chloride 7a (1069 mg, 4.648 mmol) in CH_2Cl_2 (2 mL) was added dropwise at 0 ^oC. The reaction mixture was stirred for 12 h. The reaction was then concentrated and the residue was purified on a silica gel column eluting with 50% ethyl acetate in petroleum. Yielding 76% compound 8a (1141 mg) as a white solid. Compounds 8b-c and 9a-r were synthesized following the procedure of preparation 8a.

General procedure for the synthesis of compounds 10a-r

To a solution of (S)-5-((1-methoxy-1-oxopent-4-en-2-yl)carbamoyl) benzene-1,2,3-triyl triacetate 9a (600 mg, 1.474 mmol) in a solvent of 1:1 ratio of tetrahydrofuran to methanol (6 ml) was added dropwise $NaHCO_3$ (1M, 3ml). The reaction was allowed to 3h at rt. The mixture was treated with an aqueous solution of HCl (1M) to reach pH=7. The solvent was removed using a rotary evaporator under reduced pressure. Afterwards deionized water was added and the phases were

extracted with ethyl acetate in three times. The organic layer was washed with deionized water in three times and was dried over Na_2SO_4. The solvent was removed under reduced pressure. Yielding 82% compound 10a (339 mg) as a light yellow oil. Compounds 10b-r were synthesized following the procedure of preparation 10a.

S-allyl-L-cysteine (1a)

White solid, yield: 65%. ^{1}H NMR (400 MHz, DMSO) δ 7.61 (s, 2H), 5.76 (m, , 1H), 5.13 (m, 2H), 3.30 (m, 1H), 3.17 (m, 2H), 2.95 (m, 1H), 2.67 (m, 1H). ^{13}C NMR (101 MHz, D_2O) δ 172.77, 133.45, 118.31, 53.43, 33.84, 30.65. ESI-MS: m/z calcd for $C_6H_{11}NO_2S$ ($M + H^+$) 162.3, found 162.3.

S-(prop-2-yn-1-yl)-L-cysteine (1d)

Light yellow solid, yield: 76%. ^{1}H NMR (400 MHz, D_2O) δ 3.92 (m, 1H), 3.31 (d, 2H), 3.22 (m, 1H), 3.09 (m, 1H), 2.61 (t, 1H). ^{13}C NMR (101 MHz, D_2O) δ 172.57, 79.90, 72.54, 53.22, 31.73, 18.67. ESI-MS: m/z calcd for $C_6H_9NO_2S$ ($M + H^+$) 160.5, found 160.6.

Methyl S-allyl-L-cysteinate (2a)

White solid, yield: 93%. ^{1}H NMR (400 MHz, $CDCl_3$) δ 8.77 (s, 2H), 5.88 – 5.73 (m, 1H), 5.21 (m, 2H), 4.45 (d, 1H), 3.87 (s, 3H), 3.39 – 3.05 (m, 4H). ^{13}C NMR (101 MHz, $CDCl_3$) δ 168.52, 133.21, 118.53, 53.51, 52.62, 34.93, 30.28. ESI-MS: m/z calcd for $C_7H_{13}NO_2S$ ($M + H^+$) 176.7, found 176.8.

Methyl S-(prop-2-yn-1-yl)-L-cysteinate (2d)

Brown solid, yield: 90%.^{1}H NMR (400 MHz, DMSO) δ 8.88 (s, 2H), 4.32 (t, 1H), 3.76 (s, 3H), 3.55 – 3.40 (m, 2H), 3.28 (t, 1H), 3.23 – 3.11 (m, 2H). ^{13}C NMR (101 MHz, DMSO) δ 169.00, 80.16, 74.82, 53.38, 51.81, 31.18, 19.39. ESI-MS: m/z calcd for $C_7H_{11}NO_2S$ ($M + H^+$) 174.5, found 174.5.

Methyl S-benzyl-L-cysteinate (2e)

White solid, yield: 78%. ^{1}H NMR (400 MHz, DMSO) δ 8.85 (s, 2H), 7.52 – 7.16 (m, 5H), 4.29 (s, 1H), 3.83 (d, 2H), 3.75 (s, 3H), 2.97 (m, 2H). ^{13}C NMR (101 MHz, DMSO) δ 169.03, 138.16, 129.39, 128.86, 127.49, 53.34, 52.12, 35.81, 31.21. ESI-MS: m/z calcd for $C_{11}H_{15}NO_2S$ ($M + H^+$) 226.2, found 226.3.

3,4,5-triacetoxybenzoic acid (4a)

White solid, yield: 95%. ^{1}H NMR (400 MHz, $CDCl_3$) δ 7.89 (s, 2H), 2.34 (s, 3H), 2.34 (s, 6H). ^{13}C NMR (101 MHz, $CDCl_3$) δ 169.53, 167.59, 166.37, 143.44, 139.28, 127.37, 122.77, 20.51, 20.12. ESI-MS: m/z calcd for $C_{13}H_{12}O_8$ ($M + H^+$) 297.3, found 297.4.

3,5-diacetoxybenzoic acid (4b)

White solid, yield: 91%. ^{1}H NMR (400 MHz, DMSO) δ 13.34 (s, 1H), 7.59 (d, J = 2.2 Hz, 2H), 7.28 (t, J = 2.2 Hz, 1H), 2.29 (s, 6H). ^{13}C NMR (101 MHz, DMSO) δ 169.33, 166.13, 151.30, 133.33, 120.77, 120.57, 21.19. ESI-MS: m/z calcd for $C_{11}H_{10}O_6$ ($M + H^+$) 239.3, found 239.3.

4-acetoxybenzoic acid (4c)

White solid, yield: 97%. ^{1}H NMR (400 MHz, $CDCl_3$) δ 10.85 (s, 1H), 8.18 (d, J = 8.3 Hz, 2H), 7.24 (d, J = 8.3 Hz, 2H), 2.36 (s, 3H). ^{13}C NMR (101 MHz, $CDCl_3$) δ 171.32, 168.75, 154.95, 131.81, 126.76, 121.70, 21.10. ESI-MS: m/z calcd for $C_9H_8O_4$ ($M + H^+$) 181.7, found 181.8.

Methyl S-allyl-N-(3,4,5-trimethoxybenzoyl)-L-cysteinate (8a)

White solid, yield: 76%. ^{1}H NMR (400 MHz, $CDCl_3$) δ 7.06 (s, 2H), 6.91 (d, 1H), 5.83 – 5.70 (m, 1H), 5.14 (m, 1H), 5.12 (m, 1H), 4.99 (m, 1H), 3.91 (d, 9H), 3.83 (s, 3H), 3.16 (m, 3H), 3.13 – 2.98 (m, 1H). ^{13}C NMR (101 MHz, $CDCl_3$) δ 171.45, 166.61, 153.19, 141.31, 133.45, 128.96, 117.96, 104.54, 60.85, 56.30, 52.69, 52.12, 35.10, 32.60. ESI-MS: m/z calcd for $C_{17}H_{23}NO_6S$ ($M + H^+$) 370.4, found 370.4.

Methyl S-(but-3-en-1-yl)-N-(3,4,5-trimethoxybenzoyl)-L-cysteinate (8b)

White solid, yield: 78%. ^{1}H NMR (400 MHz, $CDCl_3$) δ 7.05 (d, J = 1.7 Hz, 2H), 6.97 (d, J = 7.2 Hz, 1H), 5.78 (m, 1H), 5.09 – 4.96 (m, 3H), 3.89 (d, 9H), 3.81 (s, 3H), 3.20 – 3.07 (m, 2H), 2.61 (m, 2H), 2.33 (q, 2H). ^{13}C NMR (101 MHz, $CDCl_3$) δ 171.40, 166.66, 153.17, 141.32, 136.07, 128.95, 116.21, 104.57, 60.82, 56.28, 52.68, 52.32, 34.12, 33.66, 31.95. ESI-MS: m/z calcd for $C_{18}H_{25}NO_6S$ ($M + H^+$) 384.6, found 384.5.

Methyl S-(pent-4-en-1-yl)-N-(3,4,5-trimethoxybenzoyl)-L-cysteinate (SMU-8c)

White solid, yield: 82%. ^{1}H NMR (400 MHz, $CDCl_3$) δ 7.06 (d, J = 1.7 Hz, 2H), 6.94 (d, J = 7.3 Hz, 1H), 5.75 (m, 1H), 5.04 – 4.95 (m, 3H), 3.91 (d, 9H), 3.82 (s, 3H), 3.19 – 3.06 (m, 2H), 2.55 (t, 2H), 2.13 (q, 2H), 1.66 (q, 2H). ^{13}C NMR (101 MHz, $CDCl_3$) δ 171.42, 166.62, 153.19, 141.34, 137.32, 128.97, 115.34, 104.57, 60.83, 56.30, 52.67, 52.31, 34.11, 32.52, 32.01, 28.58. ESI-MS: m/z calcd for $C_{19}H_{27}NO_6S$ ($M + H^+$) 398.9, found 398.9.

Methyl S-(prop-2-yn-1-yl)-N-(3,4,5-trimethoxybenzoyl)-L-cysteinate (8d)

White solid, yield: 74%. ^{1}H NMR (400 MHz, $CDCl_3$) δ 7.07 (s, 2H), 6.94 (m, J = 7.3, 3.3 Hz, 1H), 5.06 (m, 1H), 3.91 (d, 9H), 3.84 (s, 3H), 3.41 – 3.32 (m, 2H), 3.32 – 3.20 (m, 2H), 2.30 (t, 1H). ^{13}C NMR (101 MHz, $CDCl_3$) δ 171.34, 166.75, 153.18, 141.32, 128.90, 104.57, 79.12, 72.08, 60.85, 56.31, 52.78, 52.10, 33.50, 19.78. ESI-MS: m/z calcd for $C_{17}H_{21}NO_6S$ ($M + H^+$) 368.3, found 368.4.

Methyl S-benzyl-N-(3,4,5-trimethoxybenzoyl)-L-cysteinate (8e)

White solid, yield: 82%. ^{1}H NMR (400 MHz, $CDCl_3$) δ 7.31 (d, J = 4.4 Hz, 4H), 7.28 – 7.22 (m, 1H), 7.05 (s, 2H), 6.85 (d, J = 7.3 Hz, 1H), 5.04 – 4.98 (m, 1H), 3.93 (s, 6H), 3.92 (s, 3H), 3.81 (s, 3H), 3.76 (s, 2H), 3.10 (m, 1H), 2.99 (m, 1H). ^{13}C NMR (101 MHz, $CDCl_3$) δ 171.42, 166.67, 153.20, 141.34, 137.48, 128.97, 128.80, 128.54, 127.23, 104.58, 60.86, 56.32, 52.71, 52.08, 36.64, 33.43. ESI-MS: m/z calcd for $C_{21}H_{25}NO_6S$ ($M + H^+$) 420.9, found 420.9.

Methyl S-(4-fluorobenzyl)-N-(3,4,5-trimethoxybenzoyl)-L-cysteinate (8f)

White solid, yield: 83%. ^{1}H NMR (400 MHz, $CDCl_3$) δ 7.28 – 7.22 (m, 2H), 7.04 (s, 2H), 6.97 (m, 2H), 6.94 – 6.82 (m, 1H), 5.02 – 4.95 (m, 1H), 3.94 – 3.88 (m, 9H), 3.79 (d, 3H), 3.72 (s, 2H), 3.06 (m, 1H), 2.95 (m, 1H). ^{13}C NMR (101 MHz, $CDCl_3$) δ 171.38, 166.64, 163.13, 160.69, 153.19, 141.40, 133.24, 133.21, 130.41, 130.33, 128.85, 115.49, 115.27, 104.60, 60.83, 56.30, 52.71, 52.06, 35.80, 33.34. ESI-MS: m/z calcd for $C_{21}H_{24}FNO_6S$ ($M + H^+$) 420.4, found 420.5.

(*R*)-5-((3-(but-3-en-1-ylthio)-1-methoxy-1-oxopropan-2-yl)carbamoyl)benzene-1, 2,3-triyl triacetate (9b)

Clear oil, yield: 73%. ^{1}H NMR (400 MHz, $CDCl_3$) δ 7.60 (s, 2H), 6.94 (d, *J* = 7.4 Hz, 1H), 5.81 (m, 1H), 5.11 – 4.97 (m, 4H), 3.82 (s, 3H), 3.17 – 3.07 (m, 2H), 2.64 – 2.59 (m, 2H), 2.35 (m, 2H), 2.32 (s, 9H). ^{13}C NMR (101 MHz, $CDCl_3$) δ 171.00, 167.50, 166.38, 164.52, 143.57, 137.62, 136.09, 131.82, 119.81, 116.27, 52.76, 52.33, 34.08, 33.61, 31.97, 20.52, 20.10. ESI-MS: m/z calcd for $C_{21}H_{25}NO_9S$ ($M + H^+$) 468.9, found 468.9.

(*R*)-5-((3-(benzylthio)-1-methoxy-1-oxopropan-2-yl)carbamoyl)benzene-1,2,3-triy l triacetate (9e)

Clear oil, yield: 79%. ^{1}H NMR (400 MHz, $CDCl_3$)δ 7.56 (s, 2H), 7.29 (d, *J* = 4.4 Hz, 4H), 7.26 – 7.18 (m, 1H), 6.88 (d, *J* = 7.5 Hz, 1H), 4.99 – 4.91 (m, 1H), 3.78 (s, 3H), 3.72 (s, 2H), 3.00 (m, 2H), 2.32 (s, 9H). ^{13}C NMR (101 MHz, $CDCl_3$) δ 171.00, 167.55, 166.42, 164.58, 143.52, 137.60, 137.47, 131.80, 128.81, 128.57, 127.24, 119.86, 52.73, 52.08, 36.62, 33.24, 20.52, 20.10. ESI-MS: m/z calcd for $C_{24}H_{25}NO_9S$ ($M + H^+$) 504.6, found 504.7.

(*R*)-5-((3-(allylthio)-1-methoxy-1-oxopropan-2-yl)carbamoyl)-1,3-phenylene diacetate (9g)

Clear oil, yield: 75%. ^{1}H NMR (400 MHz, $CDCl_3$) δ 7.52 – 7.42 (m, 2H), 7.15 (t, J = 1.9 Hz, 1H), 6.93 (d, J = 7.5 Hz, 1H), 5.82 – 5.71 (m, 1H), 5.17 (m, 1H) , 5.11 (m, 1H), 4.98 (q, 1H), 3.83 (s, 3H), 3.15 (d, J = 7.2 Hz, 2H), 3.12 – 2.98 (m, 2H), 2.33 (s, 6H). ^{13}C NMR (101 MHz, $CDCl_3$) δ 171.09, 168.65, 164.99, 151.11, 135.76, 133.42, 119.00, 118.03, 117.87, 52.74, 52.15, 35.15, 32.54, 20.97. ESI-MS: m/z calcd for $C_{18}H_{21}NO_7S$ ($M + H^+$) 396.3, found 396.3.

(*R*)-5-((1-methoxy-1-oxo-3-(prop-2-yn-1-ylthio)propan-2-yl)carbamoyl)-1,3-phenylene diacetate (9j)

Clear oil, yield: 80%. ^{1}H NMR (400 MHz, $CDCl_3$) δ 7.46 (d, *J* = 2.1 Hz, 2H), 7.14 (t, *J* = 2.1 Hz, 1H), 6.99 (d, *J* = 7.6 Hz, 1H), 5.06 (m, 1H), 3.83 (s, 3H), 3.36 – 3.30 (m, 2H), 3.29 – 3.24 (m, 2H), 2.33 (s, 6H), 2.31 (t, 1H). ^{13}C NMR (101 MHz, $CDCl_3$) δ 170.97, 168.66, 165.16, 151.10, 135.76, 118.99, 117.94, 79.15, 72.21, 52.81, 52.11, 33.58, 20.97, 19.91. ESI-MS: m/z calcd for $C_{18}H_{19}NO_7S$ ($M + H^+$) 394.1, found 394.1.

Methyl N-(4-acetoxybenzoyl)-S-allyl-L-cysteinate (9m)

White solid, White solid, yield: 80%. ^{1}H NMR (400 MHz, $CDCl_3$) δ 7.91 – 7.84 (m, 2H), 7.25 – 7.16 (m, 2H), 6.96 (d, J = 7.4 Hz, 1H), 5.84 – 5.69 (m, 1H), 5.16 (m, 1H), 5.09 (m, 1H), 5.04 – 4.97 (m, 1H), 3.82 (s, 3H), 3.15 (m, 2H), 3.12 – 2.97 (m, 2H), 2.34 (s, 3H). ^{13}C NMR (101 MHz, $CDCl_3$) δ 171.27, 168.86, 166.00, 153.36, 133.44, 131.18, 128.57, 121.80, 117.97, 52.69, 52.07, 35.12, 32.60, 21.06. ESI-MS: m/z calcd for $C_{16}H_{19}NO_5S$ ($M + H^+$) 338.9, found 338.8.

Methyl N-(4-acetoxybenzoyl)-S-(but-3-en-1-yl)-L-cysteinate (9n)

White solid, yield: 83%. ^{1}H NMR (400 MHz, $CDCl_3$) δ 7.87 (d, *J* = 8.3 Hz, 2H), 7.21 (d, *J* = 8.4 Hz, 2H), 6.99 (d, *J* = 7.4 Hz, 1H), 5.80 (m, 1H), 5.10 – 5.00 (m, 3H), 3.82 (s, 3H), 3.21 – 3.10 (m, 2H), 2.62 (t, 2H), 2.34 (m, 5H). ^{13}C NMR (101 MHz, $CDCl_3$) δ 171.23, 168.83, 166.04, 153.38, 136.08, 131.19, 128.57, 121.79, 116.24, 52.70, 52.24, 34.19, 33.66, 31.99, 21.05. ESI-MS: m/z calcd for $C_{17}H_{21}NO_6S$ ($M + H^+$) 352.3, found 352.3.

Methyl S-allyl-N-(3,4,5-trihydroxybenzoyl)-L-cysteinate (10a)

Clear oil, yield: 83%. ^{1}H NMR (400 MHz, DMSO) δ 9.13 (s, 2H), 8.73 (s, 1H), 8.44 (d, *J* = 7.7 Hz, 1H), 6.87 (s, 2H), 5.76 (m, 1H), 5.18 – 5.04 (m, 2H), 4.53 (m, 1H), 3.64 (s, 3H), 3.17 (m, 2H), 2.96 – 2.81 (m, 2H). ^{13}C NMR (101 MHz, DMSO) δ 171.93, 166.97, 145.82, 137.05, 134.58, 124.24, 117.81, 107.41, 52.67, 52.43, 34.30, 31.45. ESI-MS: m/z calcd for $C_{14}H_{17}NO_6S$ ($M + H^+$) 328.5, found 328.6.

Methyl S-(but-3-en-1-yl)-N-(3,4,5-trihydroxybenzoyl)-L-cysteinate (10b)

Clear oil, yield: 81%. ^{1}H NMR (400 MHz, DMSO) δ 9.09 (s, 2H), 8.73 (s, 1H), 8.43 (d, *J* = 7.7 Hz, 1H), 6.87 (s, 2H), 5.83 – 5.75 (m, 1H), 5.09 – 4.99 (m, 2H), 4.53 (m, 1H), 3.65 (s, 3H), 3.01 – 2.90 (m, 2H), 2.60 (t, 2H), 2.29 (m, 2H). ^{13}C NMR (101 MHz, DMSO) δ 171.97, 166.90, 145.81, 137.27, 137.01, 124.20, 116.44, 107.37, 53.03, 52.43, 33.70, 32.61, 31.04. ESI-MS: m/z calcd for $C_{15}H_{19}NO_6S$ ($M + H^+$) 342.8, found 342.9.

Methyl S-(pent-4-en-1-yl)-N-(3,4,5-trihydroxybenzoyl)-L-cysteinate (10c)

Clear oil, yield: 83%. ^{1}H NMR (400 MHz, DMSO) δ 9.09 (s, 2H), 8.82 – 8.63 (m, 1H), 8.43 (d, *J* = 7.7 Hz, 1H), 6.87 (s, 2H), 5.84 – 5.74 (m, 1H), 5.05 – 4.95 (m, 2H), 4.52 (m, 1H), 3.65 (s, 3H), 3.00 – 2.90 (m, 2H), 2.54 (d, 2H), 2.09 (m, 2H), 1.59 (q, 2H). ^{13}C NMR (101 MHz, DMSO) δ 171.98, 166.90, 145.81, 138.26, 137.01, 124.21, 115.72, 107.37, 53.07, 52.42, 32.56, 31.13, 28.55. ESI-MS: m/z calcd for $C_{16}H_{21}NO_6S$ ($M + H^+$) 356.2, found 356.3.

Methyl S-(prop-2-yn-1-yl)-N-(3,4,5-trihydroxybenzoyl)-L-cysteinate (10d)

Clear oil, yield: 79%. ^{1}H NMR (400 MHz, DMSO) δ 9.08 (s, 2H), 8.71 (s, 1H), 8.46 (d, J = 7.8 Hz, 1H), 6.86 (s, 2H), 4.59 (m, 1H), 3.66 (s, 3H), 3.40 (t, 2H), 3.21 – 3.13 (m, 2H), 3.02 (m, 1H). ^{13}C NMR (101 MHz, DMSO) δ 171.84, 166.94, 145.82, 137.05, 124.19, 107.39, 80.54, 74.32, 52.48, 52.28, 32.37, 18.96. ESI-MS: m/z calcd for $C_{14}H_{15}NO_6S$ ($M + H^+$) 326.4, found 326.5.

Methyl S-benzyl-N-(3,4,5-trihydroxybenzoyl)-L-cysteinate (10e)

Clear oil, yield: 74%. ^{1}H NMR (400 MHz, DMSO) δ 9.08 (s, 2H), 8.71 (s, 1H), 8.45 (d, J = 7.7 Hz, 1H), 7.32 (d, J = 5.2 Hz, 4H), 7.27 – 7.22 (m, 1H), 6.88 (s, 2H), 4.61 – 4.55 (m, 1H), 3.77 (s, 2H), 3.64 (s, 3H), 2.90 – 2.82 (m, 2H). ^{13}C NMR (101 MHz, DMSO) δ 171.92, 166.95, 145.82, 138.57, 137.03, 129.28, 128.79, 127.28, 124.25, 107.40, 52.59, 52.42, 35.55, 32.19. ESI-MS: m/z calcd for $C_{18}H_{19}NO_6S$ (M + H^+) 378.2, found 378.3.

Methyl S-(4-fluorobenzyl)-N-(3,4,5-trihydroxybenzoyl)-L-cysteinate (10f)

Clear oil, yield: 71%. ^{1}H NMR (400 MHz, DMSO) δ 9.10 (s, 2H), 8.74 (s, 1H), 8.47 (d, *J* = 7.7 Hz, 1H), 7.38 – 7.33 (m, 2H), 7.17 – 7.12 (m, 2H), 6.87 (s, 2H), 4.56 (m, 1H), 3.77 (s, 2H), 3.64 (s, 3H), 2.88 – 2.80 (m, 2H). ^{13}C NMR (101 MHz, DMSO) δ 171.91, 166.95, 162.74, 145.82, 137.03, 134.88, 131.21, 131.13, 124.21, 115.65, 115.44, 107.38, 52.58, 52.44, 34.66, 32.12. ESI-MS: m/z calcd for $C_{18}H_{18}FNO_6S$ (M + H^+) 396.4, found 396.5.

Methyl S-allyl-N-(3,5-dihydroxybenzoyl)-L-cysteinate (10g)

Clear oil, yield: 70%. ^{1}H NMR (400 MHz, DMSO) δ 9.49 (s, 2H), 8.63 (d, J = 7.7 Hz, 1H), 6.71 (d, J = 2.1 Hz, 2H), 6.38 (t, J = 2.2 Hz, 1H), 5.77 (m, 1H), 5.17 – 5.09 (m, 2H), 4.55 (m, 1H), 3.66 (s, 3H), 3.20 – 3.17 (m, 2H), 2.94 (m, 1H), 2.86 (m, 1H). ^{13}C NMR (101 MHz, DMSO) δ 171.70, 167.07, 158.66, 136.19, 134.63, 117.82, 106.05, 105.84, 52.65, 52.49, 34.27, 31.39. ESI-MS: m/z calcd for $C_{14}H_{17}NO_5S$ (M + H^+) 312.5, found 312.6.

Methyl S-(but-3-en-1-yl)-N-(3,5-dihydroxybenzoyl)-L-cysteinate (10h)

Clear oil, yield: 72%. ^{1}H NMR (400 MHz, DMSO-d_6) δ 9.50 (s, 2H), 8.63 (d, *J* = 7.7 Hz, 1H), 6.71 (d, *J* = 2.1 Hz, 2H), 6.38 (t, *J* = 2.2 Hz, 1H), 5.80 (m, 1H), 5.11 (m, 1H), 4.98 (m, 1H), 4.55 (m, 1H), 3.66 (s, 3H), 3.04 – 2.89 (m, 2H), 2.61 (t, 2H), 2.28 (m, 2H). ^{13}C NMR (101 MHz, DMSO) δ 171.74, 167.05, 158.66, 137.25, 136.19,

116.45, 106.03, 105.80, 53.02, 52.49, 33.69, 32.54, 31.02. ESI-MS: m/z calcd for $C_{15}H_{19}NO_5S$ ($M + H^+$) 326.8, found 326.8.

Methyl N-(3,5-dihydroxybenzoyl)-S-(pent-4-en-1-yl)-L-cysteinate (10i)

Clear oil, yield: 76%. ^{1}H NMR (400 MHz, DMSO) δ 9.50 (s, 2H), 8.62 (d, *J* = 7.7 Hz, 1H), 6.71 (d, *J* = 2.1 Hz, 2H), 6.38 (t, *J* = 2.2 Hz, 1H), 5.79 (m, 1H), 5.05 (m, 1H), 4.95 (m, 1H), 4.54 (m 1H), 3.66 (s, 3H), 2.95 (m, 2H), 2.55 (d, 2H), 2.13 – 2.05 (m, 2H), 1.60 (m, 2H). ^{13}C NMR (101 MHz, DMSO) δ 171.75, 167.04, 158.66, 138.25, 136.19, 115.72, 106.03, 105.79, 53.06, 52.48, 32.56, 32.50, 31.11, 28.55. ESI-MS: m/z calcd for $C_{16}H_{21}NO_5S$ ($M + H^+$) 340.2, found 340.3.

Methyl N-(3,5-dihydroxybenzoyl)-S-(prop-2-yn-1-yl)-L-cysteinate (10j)

Clear oil, yield: 78%. ^{1}H NMR (400 MHz, DMSO) δ 9.48 (s, 2H), 8.65 (d, *J* = 7.7 Hz, 1H), 6.71 (d, *J* = 2.2 Hz, 2H), 6.38 (s, 1H), 4.61 (m, 1H), 3.67 (s, 3H), 3.46 – 3.36 (m, 2H), 3.22 – 3.13 (m, 2H), 3.02 (m, 1H). ^{13}C NMR (101 MHz, DMSO) δ 171.61, 167.07, 158.67, 136.17, 106.04, 105.83, 80.52, 74.46, 52.63, 52.31, 32.31, 18.97. ESI-MS: m/z calcd for $C_{14}H_{15}NO_5S$ ($M + H^+$) 340.2, found 340.3.

Methyl S-benzyl-N-(3,5-dihydroxybenzoyl)-L-cysteinate (10k)

Clear oil, yield: 76%. ^{1}H NMR (400 MHz, DMSO) δ 9.49 (d, J = 1.8 Hz, 2H), 8.64 (d, J = 7.7 Hz, 1H), 7.35 – 7.21 (m, 5H), 6.72 (d, J = 2.2 Hz, 2H), 6.38 (t, J = 1.9 Hz, 1H), 4.60 (q, 1H), 3.78 (s, 2H), 3.65 (s, 3H), 2.92 – 2.81 (m, 2H). ^{13}C NMR (101 MHz, DMSO) δ 171.68, 167.09, 158.67, 138.54, 136.23, 129.27, 128.79, 127.29, 106.06, 105.83, 52.58, 52.48, 35.55, 32.16. ESI-MS: m/z calcd for $C_{18}H_{19}NO_5S$ ($M + H^+$) 362.3, found 362.3.

Methyl N-(3,5-dihydroxybenzoyl)-S-(4-fluorobenzyl)-L-cysteinate (10l)

Clear oil, yield: 74%. ^{1}H NMR (400 MHz, DMSO) δ 9.49 (s, 2H), 8.64 (d, *J* = 7.7 Hz, 1H), 7.38 – 7.34 (m, 2H), 7.17 – 7.12 (m, 2H), 6.71 (d, *J* = 2.2 Hz, 2H), 6.38 (t, *J* = 2.2 Hz, 1H), 4.58 (m, 1H), 3.78 (s, 2H), 3.65 (s, 3H), 2.89 (m, 1H), 2.83 (d, 1H).

^{13}C NMR (101 MHz, DMSO) δ 171.66, 167.09, 158.67, 131.20, 131.12, 115.65, 115.44, 106.05, 52.49, 34.68. ESI-MS: m/z calcd for $C_{18}H_{18}FNO_5S$ ($M + H^+$) 380.5, found 380.6.

Methyl S-allyl-N-(4-hydroxybenzoyl)-L-cysteinate (10m)

White solid, yield: 77%. ^{1}H NMR (400 MHz, DMSO) δ 10.03 (s, 1H), 8.60 (d, J = 7.7 Hz, 1H), 7.76 (d, J = 8.3 Hz, 2H), 6.83 (d, J = 8.3 Hz, 2H), 5.83 – 5.71 (m, 1H), 5.12 (m, 2H), 4.58 (m, 1H), 3.66 (s, 3H), 3.19 (d, 2H), 2.98 – 2.82 (m, 2H). ^{13}C NMR (101 MHz, DMSO) δ 171.91, 166.43, 160.85, 134.65, 129.84, 124.63, 117.81, 115.23, 52.68, 52.45, 34.30, 31.51. ESI-MS: m/z calcd for $C_{14}H_{17}NO_4S$ ($M + H^+$) 296.6, found 296.5.

Methyl S-(but-3-en-1-yl)-N-(4-hydroxybenzoyl)-L-cysteinate (10n)

White solid, yield: 82%. ^{1}H NMR (400 MHz, $CDCl_3$) δ 7.77 – 7.69 (m, 2H), 7.01 – 6.96 (m, 1H), 6.93 – 6.86 (m, 2H), 5.79 (m, 1H), 5.10 – 4.99 (m, 3H), 3.82 (s, 3H), 3.20 – 3.10 (m, 2H), 2.62 (t, 2H), 2.37 – 2.30 (m, 2H). ^{13}C NMR (101 MHz, $CDCl_3$) δ 171.50, 167.14, 159.75, 136.07, 129.17, 125.12, 116.27, 115.51, 52.76, 52.27, 34.21, 33.64, 31.98. ESI-MS: m/z calcd for $C_{15}H_{19}NO_4S$ ($M + H^+$) 296.5, found 296.5.

Methyl N-(4-hydroxybenzoyl)-S-(pent-4-en-1-yl)-L-cysteinate (10o)

White solid, yield: 81%. ^{1}H NMR (400 MHz, $CDCl_3$) δ 7.74 – 7.70 (m, 2H), 6.99 (d, *J* = 7.4 Hz, 1H), 6.91 – 6.87 (m, 2H), 5.75 (m, 1H), 5.00 (m, 3H), 3.82 (s, 3H), 3.19 – 3.08 (m, 2H), 2.60 – 2.50 (m, 2H), 2.17 – 2.09 (m, 2H), 1.67 (m, 2H). ^{13}C NMR (101 MHz, $CDCl_3$) δ 171.52, 167.18, 159.84, 137.35, 129.16, 125.04, 115.52, 115.36, 52.75, 52.30, 34.16, 32.52, 32.03, 28.54. ESI-MS: m/z calcd for $C_{16}H_{21}NO_4S$ ($M + H^+$) 325.2, found 325.3.

Methyl N-(4-hydroxybenzoyl)-S-(prop-2-yn-1-yl)-L-cysteinate (10p)

White solid, yield: 83%. ^{1}H NMR (400 MHz, DMSO) δ 10.03 (s, 1H), 8.62 (d, *J* = 7.8 Hz, 1H), 7.76 (d, *J* = 8.4 Hz, 2H), 6.83 (d, *J* = 8.4 Hz, 2H), 4.65 (m, 1H), 3.67 (s,

3H), 3.41 (t, 2H), 3.29 – 3.11 (m, 2H), 3.03 (m, 1H). ^{13}C NMR (101 MHz, DMSO) δ 171.82, 166.47, 160.87, 129.84, 124.59, 115.24, 80.53, 74.34, 52.51, 52.34, 32.42, 19.00. ESI-MS: m/z calcd for $C_{14}H_{15}NO_4S$ ($M + H^+$) 294.4, found 294.5.

Methyl S-benzyl-N-(4-hydroxybenzoyl)-L-cysteinate (10q)

White solid, yield: 85%. ^{1}H NMR (400 MHz, DMSO) δ 10.03 (s, 1H), 8.61 (d, J = 7.7 Hz, 1H), 7.80 – 7.74 (m, 2H), 7.34 – 7.23 (m, 5H), 6.86 – 6.80 (m, 2H), 4.68 – 4.60 (m, 1H), 3.78 (s, 2H), 3.65 (s, 3H), 2.93 – 2.82 (m, 2H). ^{13}C NMR (101 MHz, DMSO) δ 171.89, 166.46, 160.85, 138.55, 129.85, 129.27, 128.79, 127.29, 124.63, 115.23, 52.61, 52.46, 35.57, 32.25. ESI-MS: m/z calcd for $C_{18}H_{19}NO_4S$ ($M + H^+$) 346.1, found 346.2.

Methyl S-(4-fluorobenzyl)-N-(4-hydroxybenzoyl)-L-cysteinate (10r)

White solid, yield: 83%. ^{1}H NMR (400 MHz, DMSO) δ 10.03 (d, *J* = 1.2 Hz, 1H), 8.60 (d, *J* = 7.6 Hz, 1H), 7.76 (m, *J* = 8.7, 2.1 Hz, 2H), 7.37 – 7.33 (m, 2H), 7.17 – 7.12 (m, 2H), 6.83 (m, *J* = 8.7, 1.8 Hz, 2H), 4.62 (m, 1H), 3.78 (s, 2H), 3.65 (s, 3H), 2.93 – 2.81 (m, 2H). ^{13}C NMR (101 MHz, DMSO) δ 171.86, 171.64, 166.47, 162.75, 160.86, 160.34, 134.86, 134.82, 131.19, 131.11, 129.85, 124.63, 115.65, 115.44, 115.24, 52.62, 52.45, 34.73, 32.22. ESI-MS: m/z calcd for $C_{18}H_{18}FNO_4S$ ($M + H^+$) 364.2, found 364.2.

5.2. Biology assays

5.2.1. NO activation in Raw 264.7 cells

The free nitrite was monitored by using a modification of the colorimetric Griess assay. Briefly, dissolving 85% strong phosphoric acid (3 mL) and sulfanilic acid (0.5 g) in 40 mL water to make 50 mL obtained substrate solution A, then dissolving naphthyl ethylenediamine dihydrochloride (0.05 g) in 50 mL water to make substrate solution B. RAW 264.7 cells (mouse leukemic monocyte macrophage cell line) were cultured in medium of DMEM supplemented with 10% FBS, penicillin (100 U/ml),

and streptomycin (100 mg/ml), seeded in 96-well plates at 80,000 cells of density per well, and pre-incubated for 24 hours at 37°C in a 5% CO_2 humidified incubator. Removed nonadherent cells away and replaced with fresh unsupplemented DMEM medium after 24 hours incubation. The adherent macrophages were treated with 200 ng/mL Pam_3CSK_4 (InvivoGen) and different concentrations of compounds. Cells were then incubated for an additional 24 hours. After incubation, 50 μL of medium was collected to a transparent 96-well plate, then added 50 μL substrate solution A and incubated for 10 minutes in dark. After that, another 50 μL substrate solution B was added and incubated in 37 °C incubator for 10 min. Finally, absorbance was detected at 560 nm (OD560) by a microplate reader (Thermo Scientific) and afforded the content of nitric oxide by Origin 9.0 software.

5.2.2 Secreted embryonic alkaline phosphatase (SEAP) and specificity experiments.

HEK-blue hTLR2 or 3 or 4 cells (InvivoGen) were cultured in 96-well plates (4×10^4 cells per well) (Thermo Scientific) at 37°C with condition of 5% CO_2 for 24 hours on the first day in 200 μL DMEM, supplemented with 10% FBS and 1% penicillin/streptomycin. After 24 hours, nonadherent cells and medium were removed and replaced with unsupplemented fresh DMEM medium. The cells were treated with indicated concentrations of compounds and 20 ng/ml Pam_3CSK_4 (InvivoGen) in 200 μL DMEM totally. After added compounds, cells were cultured for another 24 hours. On the third day, a sample buffer (50 μL) was collected and transferred from each well of the cell culture supernatants to a transparent 96-well plate. Each well was treated with 50 μL of QUANTI-Blue (InvivoGen) buffer and incubated at 37°C in dark place. Then measure the purple color by using a plate reader at an absorbance of 620 nm (OD620) at 15-30 minutes. Finally, analyze the data by using Origin 9.0 software.

5.2.3. Cell toxicity assays

In a 96-well plate, 80,000 RAW 264.7 cells were seeded in 200 μL of growth

medium [DMEM supplemented with 10% FBS, penicillin (100 U/ml), and streptomycin (100 mg/ml)]. The plates were incubated at 37°C, 5% CO_2 for 24 hours. In the next 24 hours of treatment, the medium was changed to DMEM only and added positive control Pam_3CSK_4 (final conc. 200 ng/ml), as well as indicated concentration compounds to 200 μL totally, incubated for 24 h. Then, 20 μL (5 mg/ml in PBS) of MTT [3-(4,5-dimethylthiazol-2-yl)- 2,5-diphenyltetrazolium bromide] solution was added to each well and incubated (37°C, 5% CO_2) for another 4 hours to allow the MTT to be metabolized. The medium was removed and the plate was dried on paper towels to remove any residue. Then, 150 μL of DMSO was added in each well and shaken continuously for 40 min. When all the MTT metabolic products were dissolved, results were read by spectrophotometer at 450 nm (OD450). Optical density should be directly correlated with cell quantity.

5.2.4. Cytokine ELISA assays

Raw 264.7 cells or human PBMC cells were seeded in twelve-well plates at a density of 1×10^6 cells per well with 0.5 mL of medium DMEM medium supplemented with 10% FBS, and 1% penicillin/streptomycin. The cells were treated with indicated concentrations of SMU-8c and 50 ng/ml Pam_3CSK_4 (Invivogen) as positive control and incubated for 24 h at 37 ^oC in a 5% CO_2 humidified incubator. The cell culture supernatants were collected and frozen at -80 ^oC until measurement. THP-1 cells at a density of 2.5×10^5 cells/mL were differentiated by treatment with 100 nM PMA (Sigma) in RPMI cell culture medium, containing 10% FBS, 1% penicillin and streptomycin for 24 h at 37 °C in a 5% CO_2 humidified incubator. After that, cells were washed with PBS and cultured in fresh RPMI cell culture medium (containing 10% FBS, 1% pen/strep) for 24 h. Then, change the medium to RPMI only and treat with 50 ng/ml Pam_3CSK_4 and indicated concentration of compound for 4 hours. The cell culture supernatants were collected and froze at -80 °C until measurement. The level of cytokine TNF-α was determined using recombinant human-cytokine standards, cytokine-specific capture antibodies and detection antibodies according to the commercially available ELISA kit (BD Biosciences) with each sample for

triplicate.

5.2.5. Immunoblot analysis

In the first day, HEK-Blue hTLR2 cells were seeded in 6-well plate (Thermo Scientific) at density of 1.5×10^6 per well in 3 mL DMEM (supplemented with 10% FBS, 10 × penicillin/streptomycin, and 10 × Lglutamine) and incubated for 24 hours. In the second day, removed and replaced the medium with DMEM medium only to 3 mL totally and treated the cells with different concentration of SMU-8c and incubated for another 24 hours. In the third day, the cells were harvested and lysed with 150 μL cell lysis buffers (PIPA mixed with PMSF at ratio of 50:1 before use, Boster). Cell lysates of equal amount were denatured, separated by sodium dodecyl sulfate polycrylamide gel electrophoresis (SDS-PAGE), and transferred to nitrocellulose membrane. Then use PBS (containing 5% nonfat milk) to block the membrane for 2 h , and then incubated with the primary antibody of TLR2 overnight at 4 °C, followed with incubating by a horseradish peroxidase conjugated secondary antibody. The immunoblots were visualized by enhanced exposure machine. During the operation, the following primary and secondary antibodies were employed: mouse-GAPDH (1:2000, Solarbio, M1000110), rabbit-TLR2 (1:2000, Cell Signaling, 12276), HRP-goat-anti-mouse-IgG (1:2500, Boster, BA1050) and HRP-goat-anti-rabbit-IgG (1:1000, Boster, BA1054).

5.2.6. Immunoprecipitation assay

Human peripheral blood mononuclear cells (PBMC) with cells density of 1,000,000 cells/mL were treated with vehicle, Pam_3CSK_4 (50 ng/mL) or Pam_2CSK_4 (50 ng/mL) and indicated concentrations SMU-8c in a 6-well plate for 24 h. Cells were lysed with 200 μL lysis buffer (containing protease and phosphatase inhibitors). Then, 50 μL of the cell lysates were mixed with 1 μL of anti-TLR2 antibody and incubated overnight at 4 °C under constant rotation. To recover immunoprecipitated complexes, 10 μL of protein A agarose beads (EarthOx, nf1501) were added to the lysates and incubated for additional 4 h of incubation at 4 °C under constant rotation.

The beads were harvested by centrifugation, and the supernatant was discarded. The beads were washed with cell lysis buffers (PIPA mixed with PMSF at ratio of 50:1 before use, Boster) for three times to remove nonspecific binding protein. The beads with bound proteins were eluted by boiling in 5X SDS loading buffer at 95 °C for 5 min. The eluted proteins were subjected to electrophoresis SDS-PAGE [36]. The signals of bands were detected by probing with anti-TLR1, anti-TLR2 antibodies, anti-MyD88 antibodies, anti-TLR6 antibodies. During the operation, the following primary and secondary antibodies were employed: rabbit-TLR1 (1:2000, Cell Signaling, 2209), rabbit-TLR2 (1:2000, Cell Signaling, 12276), rabbit-TLR6 (1:1000, Proteintech, 22240-1-AP), rabbit-MyD88 (1:2000, Proteintech, 23230-1-AP) and HRP-goat-anti-rabbit-IgG (1:1000, Boster, BA1054).

5.2.7. Molecular docking modeling

Compound SMU-8c was docked into the TLR1 and TLR2 binding domain (PDB: 2Z7X) using Glide 7.4. The molecule is created, as appropriate, with multiple protonation and tautomeric states. The TLR1/2 conformations were prepared using standard Glide protocols. This includes addition of hydrogens, restrained energy-minimizations of the protein structure with the Optimized Potentials for Liquid Simulations-All Atom (OPLS-AA) force field, and finally setting up the Glide grids using the Protein and Ligand Preparation Module [37].

Acknowledgments

This work was supported by National Natural Science Foundation of China (No. 81773558 (Cheng, K), 31171281 (Chen, K)), Youth Pearl River Scholar Program of Guangdong Province (No. C1034007), Natural Science Foundation of Guangdong Province (2018B030312010), Guangdong Provincial Key Laboratory of New Drug Screening Open Fund (No. GDKLNDS-2018OF001), Major International Cooperation Projects in Universities in Guangdong Province (2015KGJHZ020), and Science and Technology Program of Guangzhou, China (201904010380).

Appendix A. Supplementary data

Supporting Information Available: Supplementary data for the representative NMR spectra associated with this article can be found in the online version at http://

References

[1] Y. Ryu, L. Jin, H.J. Kee, Z.H. Piao, J.Y. Cho, G.R. Kim, S.Y. Choi, M.Q. Lin, M.H. Jeong, Gallic acid prevents isoproterenol-induced cardiac hypertrophy and fibrosis through regulation of JNK2 signaling and Smad3 binding activity, Sci. Rep. 6 (2016) 34790. https://doi.org/10.1038/srep34790.

[2] J.H. Pang, J.H. Yen, H.T. Wu, S.T. Huang, Gallic Acid Inhibited Matrix Invasion and AP-1/ETS-1-Mediated MMP-1 Transcription in Human Nasopharyngeal Carcinoma Cells, Int J Mol Sci. 18 (2017) 1354. https://doi.org/10.3390/ijms18071354.

[3] G. Varchi, A. Battaglia, C. Samorì, E. Baldelli, B. Danieli, G. Fontana, A. Guerrini, E, Bombardelli, Synthesis of Deserpidine from Reserpine, J Nat Prod. 68 (2005) 1629-1631. https://doi.org/10.1021/np050179x.

[4] S.M. Reeve, E. Scocchera, J.J. Ferreira, N. G-Dayanandan, S. Keshipeddy, D.L. Wright, A.C. Anderson, Charged Propargyl-Linked Antifolates Reveal Mechanisms of Antifolate Resistance and Inhibit Trimethoprim-Resistant MRSA Strains Possessing Clinically Relevant Mutations, J Med Chem. 59 (2016) 6493-6500. https://doi.org/10.1021/acs.jmedchem.6b00688.

[5] S.F Nabavi, S. Tejada, W.N. Setzer, O. Gortzi, A. Sureda, N. Braidy, M. Daglia, A. Manayi and S.M. Nabavi, Chlorogenic Acid and Mental Diseases:From Chemistry to Medicine, Curr Pharm Biotechno. 15 (2017) 471-479. https://doi.org/10.2174/1570159X14666160325120625.

[6] Y.J. Chen, Y.C. Lee, C.H. Huang, L.S. Chang, Gallic acid-capped gold nanoparticles inhibit EGF-induced MMP-9 expression through suppression of p300 stabilization and NFκB/c-Jun activation in breast cancer MDA-MB-231 cells, Toxicol Appl Pharmacol. 310 (2016) 98–107. https://doi.org/10.1016/j.taap.2016.09.007.

[7] Y.J. Chen, K.N. Lin, L.M. Jhang, C.H. Huang, Y.C. Lee, L.S. Chang, Gallic acid abolishes the EGFR/Src/Akt/Erk-mediated expression of matrix metalloproteinase-9 in MCF-7 breast cancer cells, Chem Biol Interact. 252 (2016) 131–40. https://doi.org/10.1016/j.cbi.2016.04.025.

[8] J.G. LoRicco, C.S. Xu, J. Neidleman, M. Bergkvist, W.C. Greene, N.R. Roan G.I. Makhatadze, Gallic Acid Is an Antagonist of Semen Amyloid Fibrils That Enhance HIV-1 Infection, J Biol Chem. 291 (2016) 14045-14055. https://doi.org/10.1074/jbc.M116.718684.

[9] Y.Q. Liu, J.A. Carver, A.N. Calabrese, T.L. Pukala, Gallic acid interacts with α-synuclein to prevent the structural collapse necessary for its aggregation, BBA-Proteins Proteom. 9 (2014) 1481-1485.

https://doi.org/10.1016/j.bbapap.2014.04.013.
[10] C.L. Kuo, K.C. Lai, Y.S. Ma, S.W. Weng, J.P. Lin, J.G. Chung, Gallic acid inhibits migration and invasion of SCC-4 human oral cancer cells through actions of NF-κB, Ras and matrix metalloproteinase-2 and -9, Oncol Rep. 32 (2014) 355-361. https://doi.org/10.3892/or.2014.3209.
[11] C.A. Schmitt, V.M. Dirsch, Modulation of endothelial nitric oxide by plant-derived products, Nitric Oxide-Biol Ch. 21 (2009) 77-91 https://doi.org/10.1016/j.niox.2009.05.006.
[12] Y. Bansal, O. Silakari, Multifunctional compounds: Smart molecules for multifactorial diseases, Eur J Med Chem. 76 (2014) 31-42. https://doi.org/10.1016/j.ejmech.2014.01.060.
[13] Z.H. Geng, Y.Q. Rong, H.S. Lau, S-Allyl Cysteine Inhibits Activation of Nuclear Factor Kappa B in Human T Cells, Free Radic Biol Med. 23 (1997) 345-350. https://doi.org/10.1016/S0891-5849(97)00006-3.
[14] C.H. Liu, X.F. Gu, Y.Z. Zhu, Synthesis and biological evaluation of novel leonurine–SPRC conjugate as cardioprotective agents, Bioorg Med Chem Lett. 20 (2010) 6942-6946. https://doi.org/10.1016/j.bmcl.2010.09.135.
[15] C.H. Liu, W. Guo, X.R. Shi, M.A. Kaium, X.F. Gu, Y.Z. Zhu, Leonurine-cysteine analog conjugates as a new class of multifunctional anti-myocardial ischemia agent, Eur J Med Chem. 46 (2011) 3996-4009. https://doi.org/10.1016/j.ejmech.2011.05.073.
[16] Y.Y. Cheng, X.C. Li, H.F. Tse, J.H. Rong, Gallic Acid-L-Leucine Conjugate Protects Mice against LPS-Induced Inflammation and Sepsis via Correcting Proinflammatory Lipid Mediator Profiles and Oxidative Stress, Oxid Med Cell Longev. 2018 (2018) 1-14. https://doi.org/10.1155/2018/1081287.
[17] L.F. Li, K.C. Chang, Y.M. Zhou, B. Shieh, J. Ponder, A.D. Abraham, H. Ali, A. Snow, J.M. Petrash, D.V. LaBarbera, Design of an Amide N-Glycoside Derivative of β-Glucogallin: A Stable, Potent, and Specific Inhibitor of Aldose Reductase, J Med Chem. 57 (2014) 71-77. https://doi.org/10.1021/jm401311d.
[18] J. Vrba, R. Gažák, M. Kuzma, B. Papoušková, J. Vacek, M. Weiszenstein, V. Křen, J. Ulrichová, A Novel Semisynthetic Flavonoid 7-O-Galloyltaxifolin Upregulates Heme Oxygenase-1 in RAW264.7 Cells via MAPK/Nrf2 Pathway, J Med Chem. 56 (2013) 856-866. https://doi.org/10.1021/jm3013344.
[19] J.A. Jara, V.C. Castillo, J.S. Olavarría, L. Peredo, M. Pavanni, F. Jaña, M.E. Letelier, E.Parra, M.I. Becker, A. Morello, U. Kemmerling, J.D. Maya, J. Ferreira, Antiproliferative and Uncoupling Effects of Delocalized, Lipophilic, Cationic Gallic Acid Derivatives on Cancer Cell Lines. Validation in Vivo in Singenic Mice, J Med Chem. 57 (2014) 2440–2454. https://doi.org/10.1021/jm500174v.
[20] G. Nesi, Q.H. Chen, S. Sestito, M. Digiacomo, X.H. Yang, S.G. Wang, R.B. Pi, S. Rapposelli, Nature-based molecules combined with rivastigmine: A symbiotic approach for the synthesis of new agents against Alzheimer's disease, Eur J Med Chem. 141 (2017) 232-239. https://doi.org/10.1016/j.ejmech.2017.10.006.
[21] G. Deng, J. Ge, C. Liu, J. Pang, Z. Huang, J. Peng, J. Sun, J. Hou, X. Zhang, Impaired expression and function of TLR8 in chronic HBV infection and its association with treatment responses during peg-IFN-α-2a antiviral therapy, Clin Res

Hepatol Gastroenterol. 41 (2017) 386-398. https://doi.org/10.1016/j.clinre.2016.12.006.
[22] Y. Cheng, Y. Zhu, X. Huang, W. Zhang, Z. Han, S. Liu, Association between TLR2 and TLR4 Gene Polymorphisms and the Susceptibility to Inflammatory Bowel Disease: A Meta-Analysis, PLoS One. 10 (2015) : e0126803. https://doi.org/10.1371/journal.pone.0126803.
[23] X. Jing, Z.B. Tian, P.J. Gao, H.S. Xiao, X.L. Qi, Y.N. Yu, X.L. Ding, L. Yang, L. Zong, HBsAg/β2GPI activates the NFκB pathway via the TLR4/MyD88/IκBα axis in hepatocellular carcinoma, Oncol Rep. 40 (2018) 1035-1045. https://doi.org/10.3892/or.2018.6507.
[24] S. Wu, X. Lu, Z.L. Zhang, P. Lei, P. Hu, M. Wang, B. Huang, W. Xing, X.T. Jiang, H.J. Liu, Z.G. Zhu, W.H. Li, H.F. Zhu, N. Fu, G.X. Shen, CC chemokine ligand 21 enhances the immunogenicity of the breast cancer cell line MCF-7 upon assistance of TLR2, Carcinogenesis. 32 (2011) 296-304. https://doi.org/10.1093/carcin/bgq265.
[25] Q.C. Zeng, R. Song, L.H. Ao, D.L. Xu, N. Venardos, D.A. Fullerton, X.Z. Meng, Augmented osteogenic responses in human aortic valve cells exposed to oxLDL and TLR4 agonist: a mechanistic role of Notch1 and NF-κB interaction, PLoS One. 9 (2014) : e95400. https://doi.org/10.1371/journal.pone.0095400.
[26] Y. Liu, Y. Gao, X.L. Zhan, L. Cui, S.M. Xu, D.D. Ma, J. Yue, B.L. Wu, J. Gao, TLR4 Activation by Lipopolysaccharide and Streptococcus mutans Induces Differential Regulation of Proliferation and Migration in Human Dental Pulp Stem Cells, J Endod. 40 (2014) 1375-1381. https://doi.org/10.1016/j.joen.2014.03.015.
[27] Q.C. Zeng, C.H. Jin, L.H. Ao, J.C. Cleveland, R. Song, D.L. Xu, D.A. Fullerton, X.Z. Meng, Cross-Talk Between the Toll-Like Receptor 4 and Notch1 Pathways Augments the Inflammatory Response in the Interstitial Cells of Stenotic Human Aortic Valves, Circulation. 126 (2012) S222-230. https://doi.org/10.1161/CIRCULATIONAHA.111.083675.
[28] Y.S. Wang, Y. Li, Q.Y. Shen, X.P. Li, J. Lu, X.P. Li, D.L. Yin, Y. Peng, Valsartan Blocked Alcohol-Induced, Toll-Like Receptor 2 Signaling-Mediated Inflammation in Human Vascular Endothelial Cells, Alcohol Clin Exp Res. 38 (2014) 2529-2540. https://doi.org/10.1111/acer.12532.
[29] L. Gong, Y.Z. Wang, L.L. Zhou, X.Y. Bai, S. Wu, F.X. Zhu, Y.F. Zhu, Activation of Toll-like Receptor-7 Exacerbates Lupus Nephritis by Modulating Regulatory T Cells, Am J Nephrol. 40 (2014) 325-344. https://doi.org/10.1159/000368204.
[30] J.L. Li, C.H. Jin, J.C. Cleveland, L.H. Ao, D.L. Xu, D.A. Fullerton, X.Z. Meng, Enhanced inflammatory responses to toll-like receptor 2/4 stimulation in type 1 diabetic coronary artery endothelial cells: the effect of insulin, Cardiovasc Diabetol. 9 (2010) : 90. https://doi.org/10.1186/1475-2840-9-90.
[31] K. Cheng, X.H. Wang, S.T. Zhang, H. Yin, Discovery of Small-Molecule Inhibitors of the TLR1/TLR2 Complex, Angew Chem Int. 51 (2012) 12246-12249. https://doi.org/10.1002/anie.201204910.
[32] S.Y. Cai, G.Z. Zhu, X.H. Cen, J.J. Bi, J.R. Zhang, X.S. Tang, K. Chen, K. Cheng, Synthesis, structure-activity relationships and preliminary mechanism study of N-benzylideneaniline derivatives as potential TLR2 inhibitors, Bioorg Med Chem. 26

(2018) 2041-2050. https://doi.org/10.1016/j.bmc.2018.03.001.
[33] Y. Xu, S.J. Chen, Y. Cao, P.Z. Zhou, Z.P. Chen, K. Cheng, Discovery of novel small molecule TLR4 inhibitors as potent anti-inflammatory agents, Eur J Med Chem. 154 (2018) 253-266. https://doi.org/10.1016/j.ejmech.2018.05.033.
[34] Z. Chen, X. Cen, J. Yang, Z. Lin, M. Liu, K. Cheng, Synthesis of urea analogues bearing N-alkyl-N'-(thiophen-2-yl) scaffold and evaluation of their innate immune response to toll-like receptors, Eur J Med Chem. 169 (2019) 42-52. https://doi.org/10.1016/j.ejmech.2019.02.067.
[35] X. Cen, G.Z. Zhu, J.J. Yang, J.Y. Guo, J.B. Jin, K.S. Nandakumar, W. Yang, H. Yin, S.W. Liu, K. Cheng, TLR1/2 Specific Small-molecule Agonist Suppresses Leukemia cancer cell growth by stimulating Cytotoxic T lymphocytes, Adv Sci. 6 (2019) 1802042. https://doi.org/10.1002/advs.201802042.
[36] Z.F. Zhong, L.J. Liu, Z.Q. Dong, L.H. Lu, M.D. Wang, C.H. Leung, D.L. Ma, Y.T. Wang, Structure-based discovery of an immunomodulatory inhibitor of TLR1–TLR2 heterodimerization from a natural product-like database, Chem Commun. 51 (2015) 11178—11181. https://doi.org/ 10.1039/c5cc02728d.
[37] K. Cheng, X.X. Wang, H. Yin, Small-Molecule Inhibitors of the TLR3/dsRNA Complex, J Am Chem Soc. 133 (2011) 3764–3767. https://doi.org/10.1021/ja111312h.

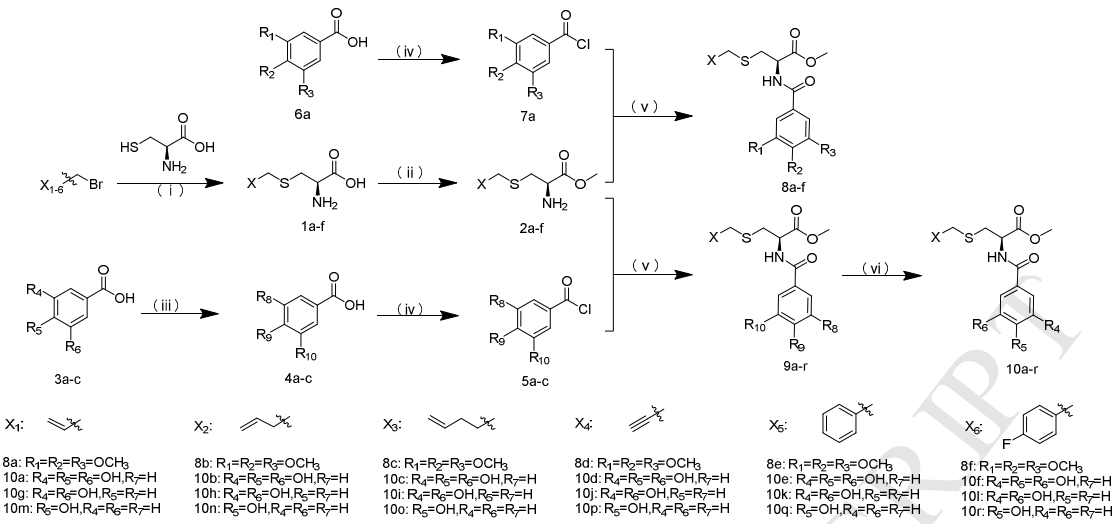

Scheme 1. Synthesis of compounds 8a-f and 10a-r. Reagents and conditions: (i) $NH_3 \cdot H_2O$, 0 ^oC, 12 h. (ii) $SOCl_2$, CH_3OH, 0 ^oC, 12 h. (iii) Acetic anhydride, rf, 4 h. (iv) $SOCl_2$, rf, 4 h. (v) Triethylamine, CH_2Cl_2, 0 ^oC, 12 h. (vi) $NaHCO_3$ (1M), THF:CH_3OH=1:1, 4 h.

Table 1. The IC_{50} values of compounds in RAW 264.7 cell.

Compound	Structure	Antagonist IC_{50} (μM)[a]	Compound	Structure	Antagonist IC_{50} (μM)[a]
1a (SAC)	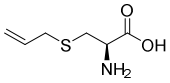	NA[b]	2e	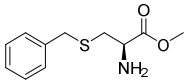	116.73±1.23
1b	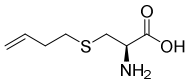	NA	2f	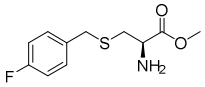	99.55±3.87
1c	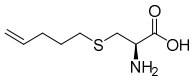	NA	3a	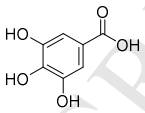	69.25±4.22
1d	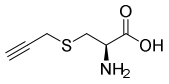	NA	3b	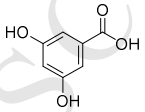	117.11±5.88
1e	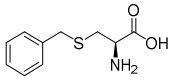	NA	3c	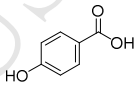	118.11±7.81
1f	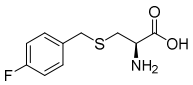	NA	6a	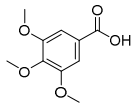	53.80±3.90
2a	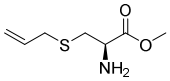	54.37±4.35	8a	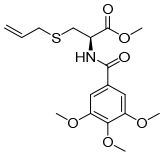	49.28±0.62
2b	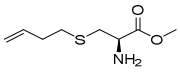	45.54±9.21	8b	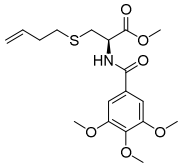	27.32±4.77
2c	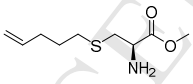	31.28±5.10	8c (SMU-8c)	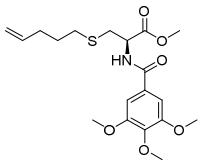	22.54±2.60
2d	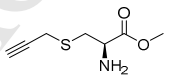	94.37±4.88	8d	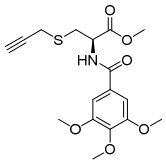	53.22±0.46

Continued Table 1. The IC_{50} values of compounds in RAW 264.7 cell.

Compound	Structure	Antagonist IC_{50} (μM)[a]	Compound	Structure	Antagonist IC_{50} (μM)[a]
8e	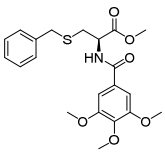	32.65±2.14	10i	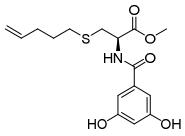	57.75±18.70
8f	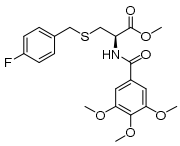	28.57±0.92	10j	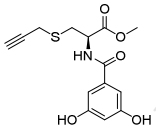	41.81±3.59
10a	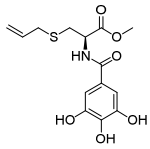	52.12±6.06	10k	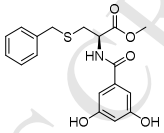	50.52±3.2
10b	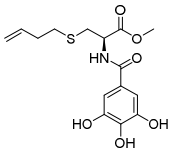	57.75±1.87	10l	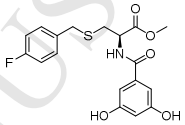	38.35±1.14
10c	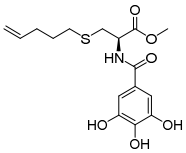	39.22±8.57	10m	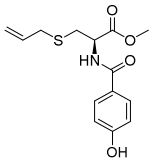	40.47±7.74
10d	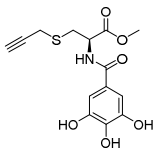	71.46±3.37	10n	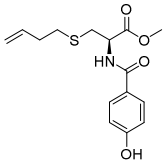	54.91±43.7
10e	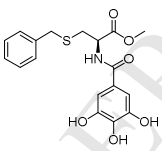	60.67±1.50	10o	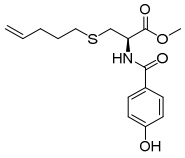	53.04±7.46
10f	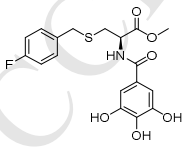	50.21±1.68	10p	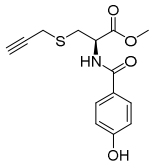	54.76±11.73
10g	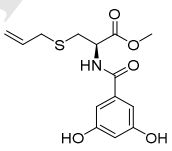	58.47±2.88	10q	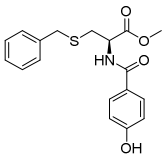	52.13±3.21
10h	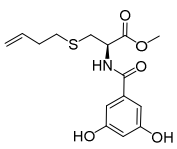	35.82±7.80	10r	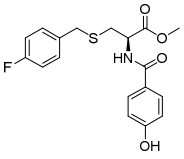	37.30±2.65

[a]Each compound was tested in triplicate. [b]NA means no activation at 150 μM.

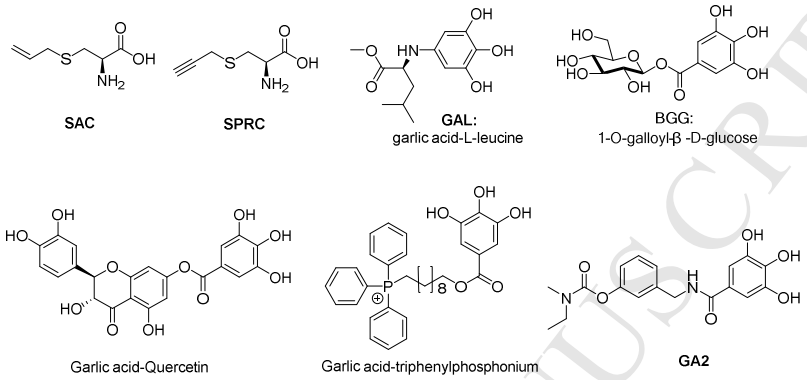

Fig. 1. Structures of SAC, SPRC and garlic acid conjugates**.**

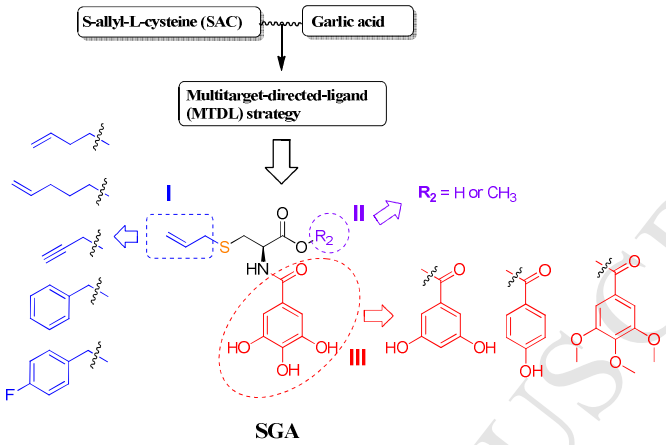

Fig. 2. The design strategy of SAC-Garlic acid (SGA) conjugates.

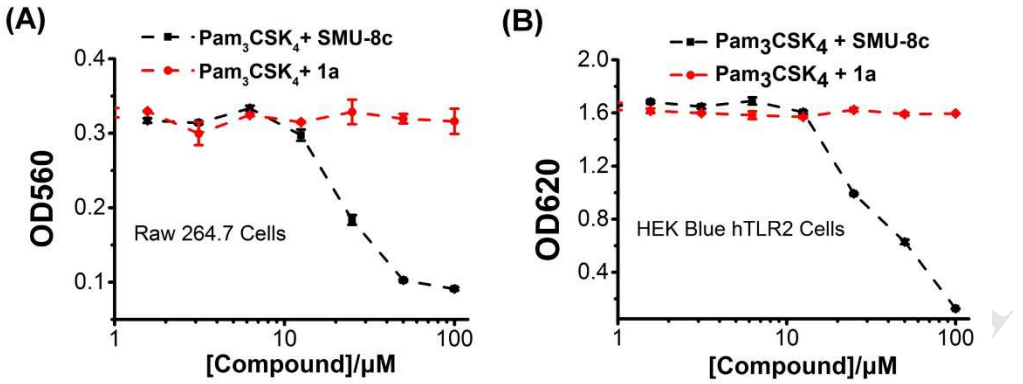

Fig. 3. **Compare of SMU-8c and 1a in the inhibition of inflammatory cytokines**. (A) RAW 264.7 cells were treated with 200 ng/ml Pam_3CSK_4 and indicated concentration of compound for 24 hours. The nitric oxide (NO) signaling was detected by Griess method in the culture supernatants at OD560. (B) Comparison of SMU-8c and 1a inhibited secreted embryonic alkaline phosphatase (SEAP) signals in HEK-Blue hTLR2 cells. HEK-Blue hTLR2 cells were incubated with Pam_3CSK_4 (100 ng/mL) together with SMU-8c or 1a for 24 hours, and the activation was measured by Quanti-Blue in the culture supernatants at OD620.

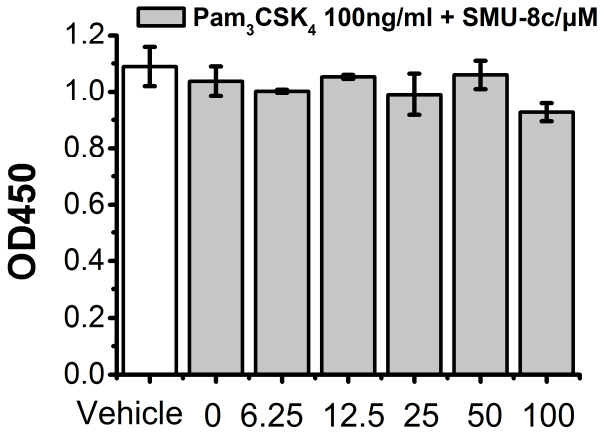

Fig. 4. Cytotoxicity of SMU-8c was tested by MTT colorimetric method in RAW 264.7 cells. RAW 264.7 macrophage cells were cultured in DMEM at 37 °C for 24 hours before drug treatment. Indicated concentration compounds were added and incubated at 37 ^{o}C for another 24h. The cell viability was detected through MTT at OD450. Data presented are mean ± SD and the figures shown are representative of three independent experiments.

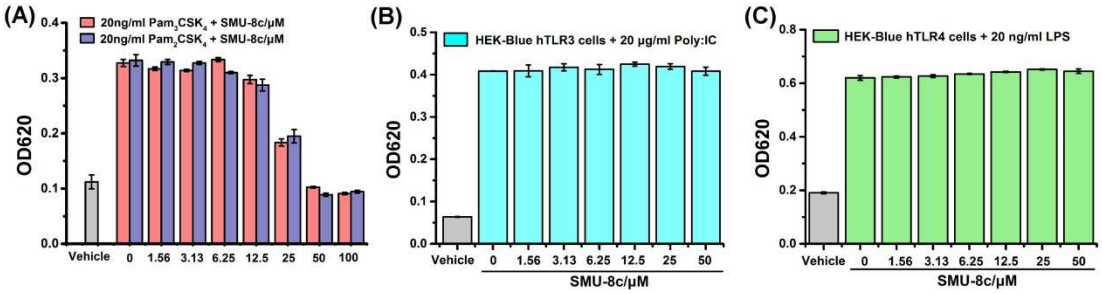

Fig. 5. Specificity test for SMU-8c in HEK-Blue hTLR2, 3 and 4 cells. (A) HEK-Blue hTLR2 cells were incubated with SMU-8c (0-100 μM) with 20 ng/ml Pam_3CSK_4 or 20 ng/ml Pam_2CSK_4 as the positive ligand of TLR 1/2 or TLR 2/6, respectively. (B and C) HEK-Blue hTLR3 (B) or 4 (C) cells were treated with SMU-8c (0-50 μM) with 20 μg/ml Poly:IC or 20 ng/ml LPS as the positive control, the vehicle as the neagtive control. Data presented are mean ± SD and the figures shown are representative of three independent experiments.

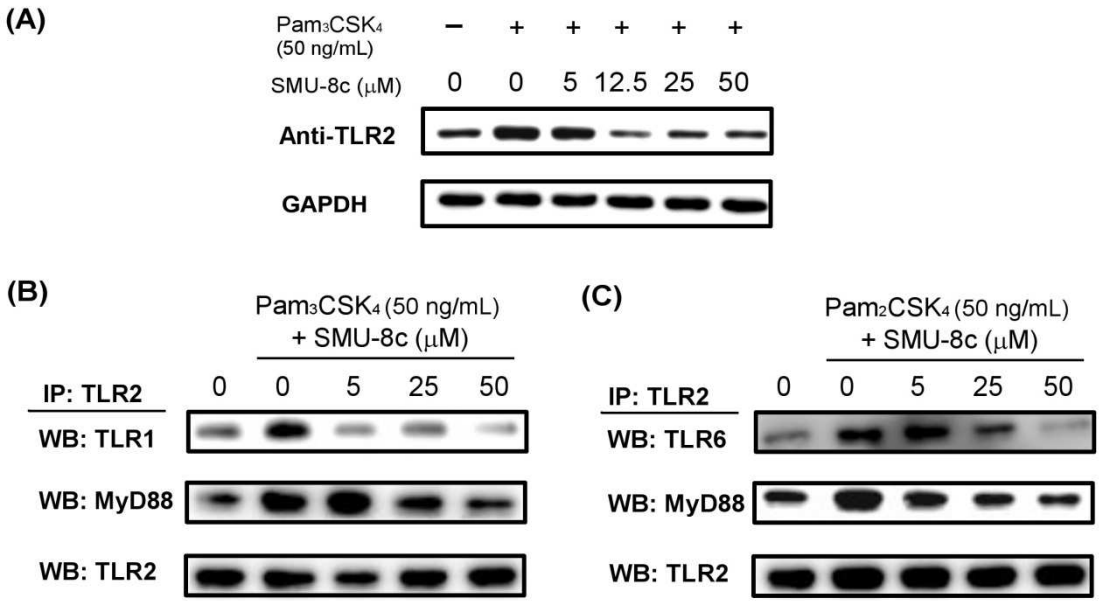

Fig. 6. The inhibit effect of compound SMU-8c on TLR1/2, TLR2/6 and TLR2/MyD88. (A) Western Blot experiment indicated SMU-8c can inhibit the Pam_3CSK_4 (50 ng/mL) upregulated TLR2 in HEK-Blue hTLR2 cells. (B) Co-immunoprecipitation showing compound SMU-8c inhibits the formation of TLR1-TLR2, TLR2-MyD88 complex in Pam_3CSK_4-stimulated human peripheral blood mononuclear cells (PBMC). (C) Compound SMU-8c inhibits the formation of TLR2-TLR6, TLR2-MyD88 complex in Pam_2CSK_4-stimulated human PBMC as determined by an immunoprecipitation experiment.

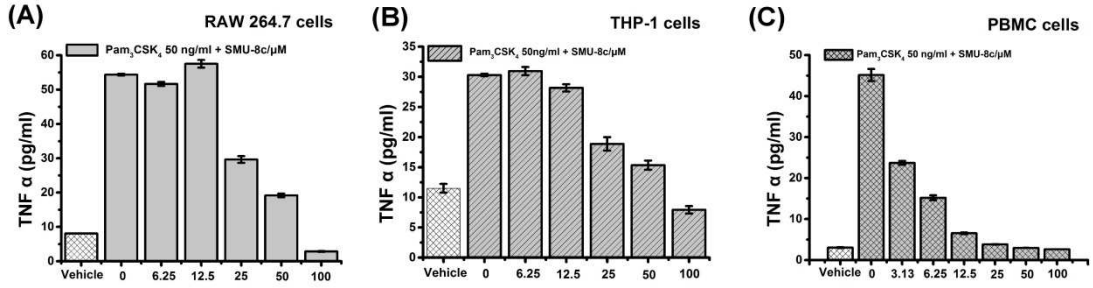

Fig. 7. SMU-8c inhibits Pam_3CSK_4 triggered TNF-α in mouse and human cells. (A) The TNF-α in the supernatants of mouse RAW 264.7 cells after treatment with SMU-8c for 24 h. (B) The TNF-α in the supernatants of human THP-1 cells after treatment with SMU-8c for 4 h. (C) The TNF-α signaling in human primary PBMC cells were test in the supernatants after treatment with SMU-8c for 24 h. Data presented are mean ± SD and the figures shown are representative of three independent experiments.

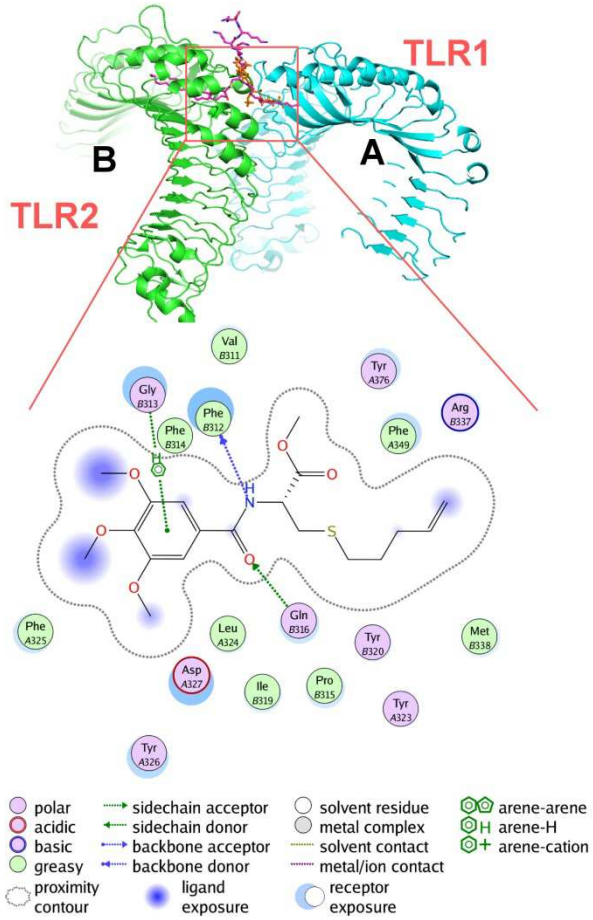

Fig. 8. Low-energy binding conformations of SMU-8c (orange) and Pam_3CSK_4 (purple) bound to the TLR1–TLR2 interface (PDB 2Z7X) as generated by virtual ligand docking. A partial enlargement shows that SMU-8c has strong hydrogen bonding with key residues Gly313 and Gln316 of TLR1 (Chain A), and hydrophobic interaction with Phe349 on TLR2 (Chain B).

Highlights for this paper

- Novel SAC-Garlic Acid natural product conjugates were designed and synthesized.
- The optimized compound SMU-8c exhibit potent inhibition to TLR2, not TLR3 and TLR4.
- SMU-8c inhibited the formation of TLR1-TLR2, and TLR2-TLR6 complex in human PBMC.
- SMU-8c provides a novel molecule probe for anti-inflammatory applications.